PAPER

Analysis of calibration-free wavelength-scanned wavelength modulation spectroscopy for practical gas sensing using tunable diode lasers

To cite this article: K Sun *et al* 2013 *Meas. Sci. Technol.* **24** 125203

Meas. Sci. Technol. **24** (2013) 125203 (12pp) doi:10.1088/0957-0233/24/12/125203

Analysis of calibration-free wavelength-scanned wavelength modulation spectroscopy for practical gas sensing using tunable diode lasers

K Sun, X Chao, R Sur, C S Goldenstein, J B Jeffries and R K Hanson

High Temperature Gasdynamics Laboratory, Department of Mechanical Engineering, Stanford University, Stanford, CA 94305, USA

E-mail: kaisun@stanford.edu

Received 16 July 2013, in final form 19 September 2013
Published 29 October 2013
Online at stacks.iop.org/MST/24/125203

Abstract

A novel strategy has been developed for analysis of wavelength-scanned, wavelength modulation spectroscopy (WMS) with tunable diode lasers (TDLs). The method simulates WMS signals to compare with measurements to determine gas properties (e.g., temperature, pressure and concentration of the absorbing species). Injection-current-tuned TDLs have simultaneous wavelength and intensity variation, which severely complicates the Fourier expansion of the simulated WMS signal into harmonics of the modulation frequency (f_m). The new method differs from previous WMS analysis strategies in two significant ways: (1) the measured laser intensity is used to simulate the transmitted laser intensity and (2) digital lock-in and low-pass filter software is used to expand both simulated and measured transmitted laser intensities into harmonics of the modulation frequency, WMS-nf_m ($n = 1, 2, 3, \ldots$), avoiding the need for an analytic model of intensity modulation or Fourier expansion of the simulated WMS harmonics. This analysis scheme is valid at any optical depth, modulation index, and at all values of scanned-laser wavelength. The method is demonstrated and validated with WMS of H_2O dilute in air (1 atm, 296 K, near 1392 nm). WMS-nf_m harmonics for $n = 1$ to 6 are extracted and the simulation and measurements are found in good agreement for the entire WMS lineshape. The use of $1f$-normalization strategies to realize calibration-free wavelength-scanned WMS is also discussed.

Keywords: laser absorption, wavelength modulation spectroscopy, calibration-free, multiple harmonics

(Some figures may appear in colour only in the online journal)

1. Introduction

Tunable diode laser absorption spectroscopy (TDLAS) is an established method for *in situ*, non-intrusive, monitors of gas composition, temperature, pressure and velocity [1–8]. With the emergence of reliable, room temperature, narrow-linewidth, wavelength-tunable diode lasers (TDLs), such absorption sensors, have transitioned in the past two decades from laboratory sensors into practical devices for industrial facilities [9–15]. Wavelength modulation spectroscopy (WMS) and direct absorption (DA) are the two most common methods for TDLAS sensing.

In DA, the laser wavelength is typically scanned across an isolated transition and the non-absorbing transmitted intensity (often called the baseline intensity) is determined by extrapolating the laser intensity from the non-absorbing regions at the extremes of the scan to account for laser intensity variation with wavelength. This baseline (incident) intensity and the transmitted intensity are combined with the Beer–Lambert relation to determine the transition lineshape

and the integrated absorbance. For homogeneous gases the interpretation of DA data is quite straightforward, as the integrated absorbance depends only on the line strength of the transition, temperature, pressure, absorber mole fraction and pathlength. DA is the method of choice for systems with isolated transitions of sufficient strength (i.e. high signal-to-noise (SNR) measurements of the absorption attenuation of the transmitted intensity) and a transition linewidth small enough to allow the laser to be wavelength-scanned on/off the absorption transition.

By contrast, the WMS method is advantageous for applications with small absorbance, high pressure or for absorbers with closely spaced transitions, which are blended in the wings precluding measurement of a non-absorbing baseline. In WMS, the laser wavelength is modulated at frequency f_m and signals are detected at the harmonics nf_m, isolating the signal from low-frequency noise [16–19]. The majority of WMS applications involve the detection of trace quantities of the target species with very small absorption signal. Except for the first harmonic, the WMS signals are ideally detected against a zero or near-zero background, while DA is detected as the difference between transmitted intensity with and without absorption. Thus, the WMS SNR is improved compared to DA by the ability to detect a small signal against a near-zero background at detection frequencies well above low-frequency intensity noise. In addition, detection of the transmitted intensity synchronously with modulation also provides WMS immunity from optical emission from the measurement volume (although for highly luminous applications care must be taken to insure the detector is not saturated).

The WMS signals at all of the harmonics are proportional to laser intensity, and the WMS signal at $1f_m$ is dominated by the intensity modulation from injection-current-modulated TDLs. Thus normalizing the WMS-nf_m signals by the WMS-$1f_m$ signal can account for variations in laser intensity, including non-absorption losses such as light scattering or beam steering [20–26]. This normalization enables quantitative WMS absorption measurements without determining a zero-absorption baseline [24, 25], making wavelength-scanned, $1f_m$-normalized WMS-nf_m an attractive strategy for absorption measurements in harsh (i.e. high-pressure, high-opacity, high-emission, high-temperature) environments, especially where the laser cannot be tuned to a non-absorbing wavelength.

The WMS absorption signal is the product of terms proportional to absorbance and the lineshape of the absorbing transition convoluted with the modulation. Thus, the analysis of WMS absorption is more complex than DA. Traditional simulation of the WMS absorption signal [27–31] uses the Beer–Lambert relation to combine an analytic model of the modulation of wavelength (and intensity) with a simulated absorption spectrum to calculate WMS-nf_m harmonics via Fourier expansion. Unfortunately, injection-current-modulated TDLs have simultaneous intensity modulation requiring an additional analytic model of the TDL intensity versus time. Thus, the Fourier expansion becomes quite complicated when the simultaneous modulation of laser intensity and wavelength are combined with a realistic absorption lineshape [32–34]. There is a large literature of analytic models that simulate WMS spectra; however, almost all these models are restricted by simplifying assumptions. For example, some models are valid only when the intensity modulation can be neglected [16], the modulation depth is small [31], or the modulation frequency is low [22]. Others are only accurate when the intensity modulation is linear, and may not be suitable for external-cavity lasers where the nonlinearity in intensity modulation can be large [35]. Related work in our laboratory [21] accounted for nonlinear modulation of the laser and the finite phase shift between intensity and wavelength modulation in its analysis of optically thin WMS at transition line center. Later this work was expanded to calibration-free measurements with larger optical depth [25]. These models become even more complex when the optical system has additional wavelength-dependent intensity variations (e.g., wavelength-dependent transmission interference (etalons) or the use of a semiconductor optical amplifier with wavelength-dependent gain to increase the laser power). Such difficulties are even more pronounced for wavelength-scanned WMS where the laser-dynamics of injection-current-tuned TDLs cannot be accurately described by a Fourier series of a single modulation frequency [36].

However, wavelength-scanned WMS is crucial for practical TDL sensors. A wavelength-scanned approach is needed to avoid problems of a drift of the mean laser wavelength with time, where the mean wavelength is defined as the center wavelength of the modulating laser. Such drifts move fixed-wavelength WMS measurements off the line center of the transition. Without independent calibration or wavelength monitoring, such drifts produce unacceptable uncertainty for a practical fixed-wavelength WMS sensor. In addition, wavelength-scanned WMS can be used to measure velocity and/or pressure (via transition lineshape) [36, 37].

Here we present a new comprehensive and accurate approach to analyze wavelength-scanned WMS absorption signals at all the harmonics of the modulation frequency. The new method differs from previous WMS analysis strategies in two significant ways: (1) the measured intensity versus time of the wavelength-scanned (at frequency f_s), wavelength-modulated (at f_m) laser light is used to simulate the transmitted laser intensity versus time, and (2) digital lock-in and low-pass filter software is used to expand the time series of simulated and measured transmitted laser intensity into harmonics of the modulation frequency, WMS-nf_m ($n = 1, 2, 3, \ldots$). Using the measured laser intensity of the scanned and modulated laser avoids the need to develop an analytic model to describe the variation of laser intensity versus time. However, the wavelength variation of the scanned and modulated laser versus time is characterized prior to measurements, similar to the traditional analysis. The use of the lock-in and filter software to expand the WMS signal into modulation frequency harmonics avoids the difficulties in the Fourier expansion of the time-varying laser intensity. The new analysis scheme is valid at any optical depth, modulation index (defined by the ratio of the wavelength modulation depth and the half width of the transition lineshape), and at all values of the mean

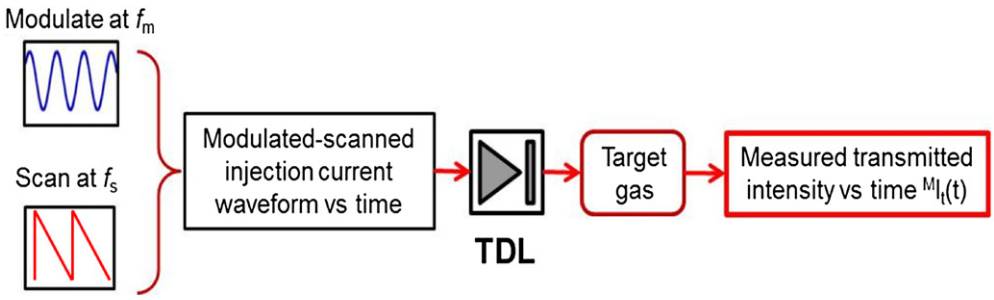

Figure 1. Measurement step: determine measured transmitted intensity versus time with absorber ${}^{M}I_t(t)$ and without absorber ${}^{M}I_0(t)$.

laser wavelength. This enables the WMS-nf_m lineshape to be fit to determine gas properties such as absorber concentration, temperature and pressure via the collision broadened linewidth [37].

The details of the analysis scheme are described in this paper in the context of a demonstration experiment to measure WMS absorption of H_2O dilute in air, in a cell at room temperature and atmospheric pressure. First, in section 2, an overview of the measurement and simulation of WMS-nf_m is provided. Then, in section 3, the details of the experiment and data analysis are discussed. The laser characterization and measurements conducted prior to the WMS experiment are described and examples of the data for the demonstration experiment are used for illustration. The absorption spectrum of the target species is simulated and then the laser characterization data are used to simulate the experiment using the Beer–Lambert relation to calculate the transmitted laser intensity for the modulated and scanned laser. Then a digital lock-in software is used to expand both measured and simulated transmitted intensity into the WMS-nf_m harmonics for $n = 1$–6. Finally, the use of $1f_m$-normalization is shown to account for non-absorption losses. The measured and simulated lineshapes agree for $1f_m$-normalized WMS-nf_m signals for $n = 2$–6 without any calibration or adjustable parameters, providing the ability to use this new WMS analysis scheme for calibration-free extraction of gas parameters from best fit analysis of WMS lineshapes [37].

Compared to past WMS analysis strategies, this new method is much easier to implement. The use of the digital lock-in and low-pass filter software to extract the WMS-nf_m harmonics from the simulated transmitted intensity avoids the complex Fourier expansion of the simulated absorption of the scanned and modulated laser intensity and wavelength. This new scheme is valid for all WMS-nf_m harmonics, at any optical depth, and at all values of the mean laser wavelength even in the wings of the absorption away from line center. In addition, this WMS analysis scheme does not require an isolated transition as it recovers the lineshape for absorption from unresolved blended transitions.

2. Overview of a WMS absorption experiment

The WMS experiment and data analysis consists of five steps: (1) measurement of the transmitted intensity of the scanned and modulated laser through the target gas sample, (2) characterization of the laser wavelength and intensity versus time in response to the time-varying laser-injection current, (3) simulation of the absorption spectrum using the characterization data and the Beer–Lambert relation to calculate the simulated transmitted intensity versus time, (4) expansion of the simulated and measured transmitted laser intensity versus time into harmonics of the WMS signal using the same lock-in and low-pass filter software, and (5) normalization of the harmonics of the WMS signal by the $1f_m$-harmonic exploiting the intensity variation of injection-current-modulated TDLs to account for non-absorption losses. The measurement and the characterization can be performed in either order, afterwards the other three steps must occur in the order listed. Research is underway to develop fitting strategies for the WMS-nf_m lineshapes and understand the role of modulation depth to optimize the extraction of gas parameters from wavelength-scanned, $1f_m$-normalized WMS measurements [37].

2.1. Transmitted intensity measurement

The measurement of the transmitted intensity of a scanned and modulated laser is illustrated in the diagram of figure 1. The TDL injection-current is rapidly modulated at frequency f_m superimposed upon a slow scan of the mean injection-current of the modulated laser at frequency f_s. In this paper superscript M and S will distinguish the time-dependent measured transmitted intensity ${}^{M}I_t(t)$ from the simulated transmitted intensity ${}^{S}I_t(t)$ by superscripts, where the subscript 't' denotes transmission through the absorbing gas, and the subscript '0' will denote the intensity measured without absorber present ${}^{M}I_0(t)$. Ideally the intensity versus time would be measured with absorber ${}^{M}I_t(t)$ and without absorber ${}^{M}I_0(t)$; however some applications do not lend themselves to an *in situ* measurement without absorber, and the ${}^{M}I_0(t)$ must be determined during the laser characterization.

2.2. Laser characterization (intensity and wavelength versus time)

The laser intensity versus time without absorbers ${}^{M}I_0(t)$ is measured at the same digitizer rate as the WMS measurements avoiding the need to model the laser intensity response with injection-current. The best intensity versus time characterization is the *in situ* measurement using the application test volume evacuated or purged of the absorbing gas discussed in section 2.1 above. However, for

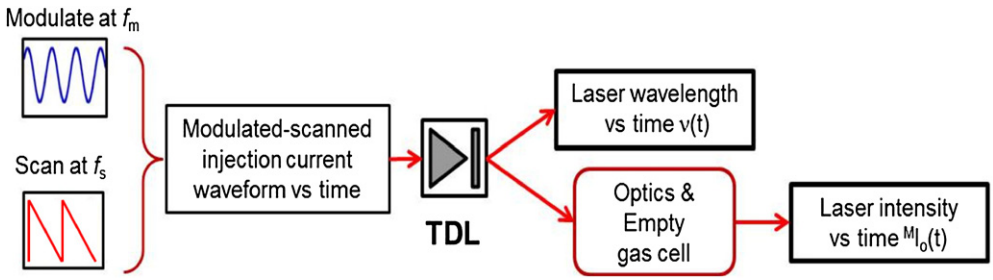

Figure 2. Wavelength characterization versus time $\nu(t)$ and intensity versus time $^{M}I_0(t)$ of a wavelength-scanned, wavelength-modulated laser including wavelength-dependent transmission along the measurement path without absorption.

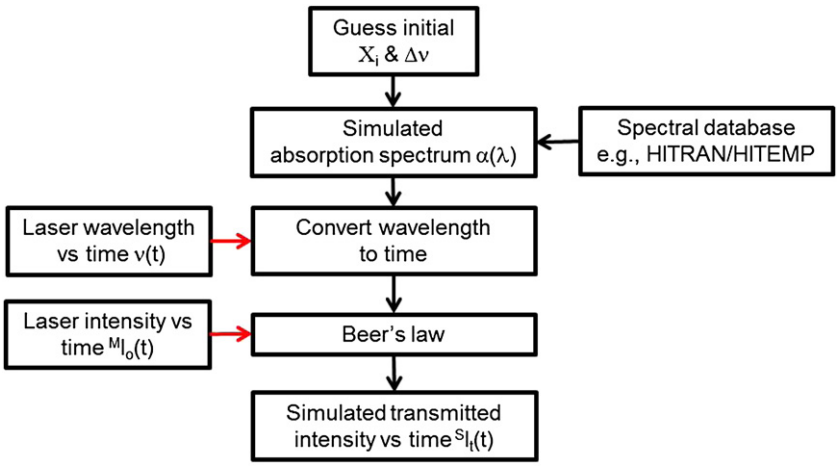

Figure 3. Simulation of transmission intensity versus time of a wavelength-scanned wavelength-modulated laser through a simulated absorption spectrum.

some practical implementations, an *in situ* absorption-free background measurement of laser intensity is not possible; successful measurements have been performed in such applications by laboratory characterization of the intensity including as many of the field measurement optics and windows as possible. When the actual field measurement is performed care in alignment and set up is taken to minimize any wavelength-dependent transmission. The dominant time variation of the laser intensity is produced by the time-varying injection-current; however additional time-varying intensity contributions can arise from the wavelength tuning (and modulation) if any optics or windows have wavelength-dependent transmission (e.g., a material near the edge of its transmission range, or more likely interference from components with parallel surfaces (etalons).

The performance of the laser tuning is characterized to determine an analytic expression for the laser wavelength versus time $\nu(t)$ as the injection-current of the laser is driven by a combination of the scan and modulation frequencies, as shown in figure 2. $\nu(t)$ is determined from a combination of measurements using an etalon and absorption transitions of known wavelength as a function of injection-current, and these data are fit to a model of the wavelength tuning.

2.3. Simulated transmitted laser intensity

The simulation of the transmitted laser intensity is illustrated in the flow chart in figure 3. First a spectral database such as HITRAN or HITEMP [38] is used to determine the absorption spectrum $\alpha(\nu)$ near the target transition for an approximate gas composition illustrated in the figure as initial guesses, a prelude to iterative fitting of the WMS lineshapes; the collision broadening in the database is used to estimate the linewidth $\Delta\nu$ of the transitions scanned. Note that the WMS analysis scheme developed here can be used for isolated transitions or multiple transitions even if they are unresolved and/or blended by collision broadening. The characterization of the laser tuning versus time $\nu(t)$ is used to convert the absorbance spectrum $\alpha(\nu)$ to an absorbance time series $\alpha(\nu(t))$. The laser intensity versus time $^{M}I_0(t)$ is combined with the absorbance time series $\alpha(\nu(t))$ using the Beer–Lambert relation to calculate the simulated transmitted laser intensity versus time $^{S}I_t(t)$ for the same time steps as the measured transmitted intensity, $^{M}I_t(t)$.

2.4. Lock-in analysis

Both the measured transmitted intensity versus time $^{M}I_t(t)$ and the simulated transmitted intensity versus time $^{S}I_t(t)$ are processed with a digital lock-in and a low-pass filter to isolate the WMS signals at the harmonics of f_m (see figure 4). The lock-in analysis of the simulated transmitted intensity extracts the WMS-nf_m harmonics while avoiding the complex mathematics of a Fourier expansion of simultaneous wavelength and intensity modulation. Nonlinear laser response to the injection-current variation for the intensity and/or laser

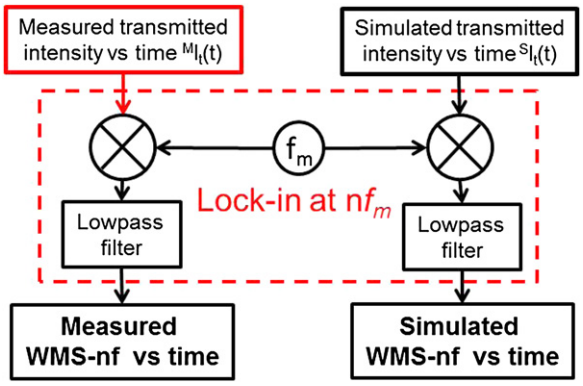

Figure 4. Use of a digital lock-in and low-pass filter to expand the time series of measured or simulated laser intensity into the WMS-nf_m harmonic signals.

wavelength can produce a background signals at the WMS-nf_m harmonics [24] (in some cases, for example, when some optical components are heated, the background signal can drift with time, but we have neglected this issue in the current paper). Using the same lock-in analysis of the simulated and measured transmitted intensity avoids explicitly evaluating these background signals as their contribution is equally included in the simulated and measured WMS-nf_m harmonics signals. Because these background signals are proportional to the laser intensity, the normalization of the WMS harmonics by the WMS-$1f_m$ signal can be performed without explicit background corrections.

2.5. Normalization to account for non-absorption losses

All of the harmonics of the WMS signal are proportional to the laser intensity. For optically thin conditions, the WMS-$1f_m$ is dominated by the injection-current modulation and it has long been recognized [20–26] that other WMS harmonics could be $1f_m$-normalized at line center to account for non-absorption losses in transmitted laser intensity. The wavelength-scanned WMS-$1f_m$ signal has a large contribution from the laser intensity modulation and contributions from gas absorption with lineshapes asymmetric ('dispersion-like') and symmetric (absorption) with respect to the transition line center. At line center the 'dispersion-like' contribution vanishes and $1f_m$-normalization of WMS-nf_m harmonics is easily understood. However, the magnitude of the asymmetric contribution is also proportional to laser intensity, and although normalization by the wavelength-scanned WMS-$1f_m$ distorts the WMS-nf_m lineshapes this normalization can still be used to account for non-absorption losses in transmitted laser intensity as the distortion is identical for measurement and simulation of the WMS signals.

3. Example analysis of WMS absorption detection of H_2O

A step-by-step discussion of the measurement and analysis of WMS absorption for an example problem, of H_2O dilute in air, provides the context for a detailed description of this new WMS analysis scheme.

3.1. Transmitted intensity measurement for WMS detection of H_2O

The example experiment was conducted with known amounts of H_2O dilute in air at atmospheric pressure as illustrated in figure 5. A DFB laser (NEL) near 1392 nm with single-mode fiber output was used to probe the H_2O transition near 7185.6 cm^{-1}. Computer driven outputs (National Instruments PCI-6110) controlled the diode laser injection-current (ILX Lightware LD-3900). The injection-current was modulated with a sine function at $f_m = 10$ kHz superposed on a linear scan $f_s = 25$ Hz. The light exiting the fiber was collimated into a beam, directed through a gas cell with wedged windows to avoid etalon interference in the transmission of the wavelength-scanned (and modulated) light. The transmitted light was then focused onto a near-infrared (NIR) photodiode detector (Thorlab PDA-10CS, bandwidth: 775 kHz at 30 dB gain). The laser intensity signal was sampled (same PCI-6110 card, 12 bits) at a rate of 2.5 MHz. The optical path external to the cell was purged with pure N_2 to eliminate the absorbance in the ambient environment. The measured transmitted intensity versus time $^{M}I_t(t)$ was acquired for H_2O dilute in air in the cell.

3.2. Laser characterization for WMS detection of H_2O

The laser intensity versus time $^{M}I_0(t)$ including any losses or wavelength variation in the optical components was then measured in the evacuated cell as illustrated in figure 6.

Characterizing the laser wavelength tuning $\nu(t)$ is more complex. First the scan-current of the modulating laser was recorded for the peak WMS-$2f_m$ signal from a selected transition. The known position of this transition was used to calibrate the absolute wavelength for the scan of the modulating laser. The wavelength tuning of the modulated laser around this calibration point was measured using a fiber input/output etalon with 0.02 cm^{-1} FSR (Micron Optics).

$\nu(t)$ is modeled as: $\nu(t) = \bar{\nu} + a\cos(2\pi f_m t + \varphi_\nu) + F(t)$, (1)

where $\bar{\nu}$ is the laser wavelength (or laser frequency) without injection-current-tuning, f_m the modulation frequency, a (cm^{-1}) the modulation depth (here 0.081 cm^{-1}), φ_ν the phase of the frequency modulation (here −2.048 radian), $F(t)$ the function describing the wide near-linear scan of the mean laser wavelength, expressed here as a fourth-order polynomial. The measured frequency-tuning response is shown in figure 7 and the best-fit result for the specific laser used in the demonstration was

$$\begin{aligned}\nu(t)(\mathrm{cm}^{-1}) &= 7182.159 + 1.3775\times10^{2}\cdot t \\ &\quad + 2.4977\times10^{3}\cdot t^{2} - 1.1702\times10^{5}\cdot t^{3} \\ &\quad + 1.3699\times10^{6}\cdot t^{4} \\ &\quad + 0.081\times\cos(2\pi\cdot10^{4}\cdot t - 2.0483).\end{aligned} \quad (2)$$

3.3. Simulated transmitted laser intensity for WMS detection of H_2O

Single-mode DFB TDLs have very narrow (∼5 MHz) linewidth and thus the Beer–Lambert relation describes the

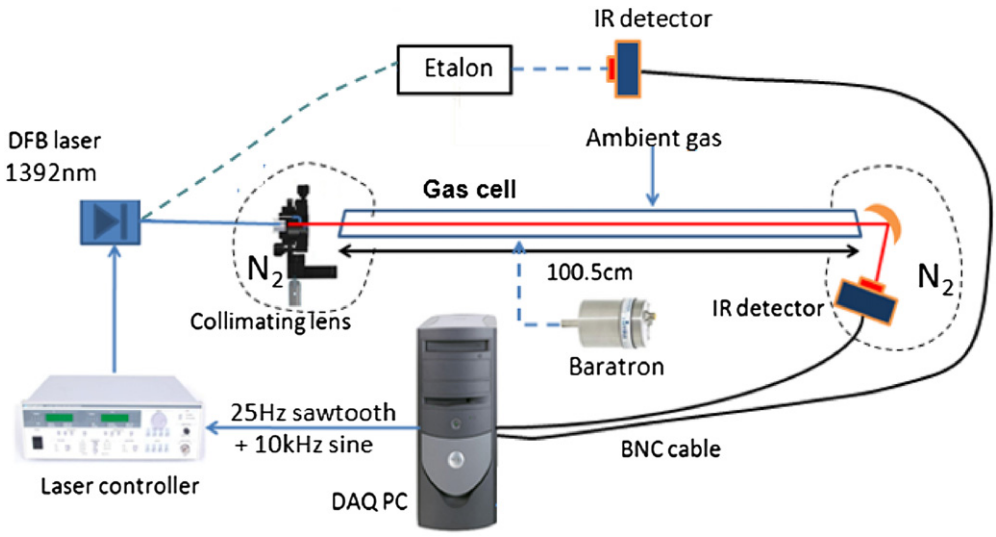

Figure 5. Schematic of the experimental setup for measuring the transmitted laser intensity versus time for WMS detection of H_2O in a gas cell.

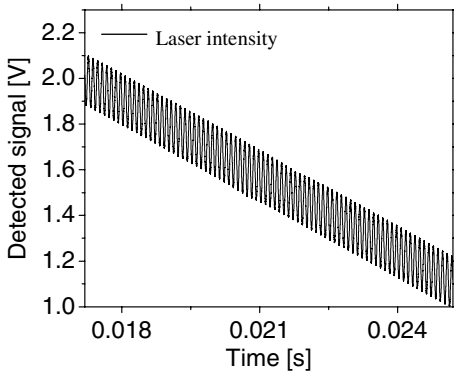

Figure 6. Measured laser intensity versus time in the absence of the absorber (scan rate = 25 Hz, scan amplitude = 2 V, modulation frequency = 10 kHz, modulation amplitude = 0.1 V).

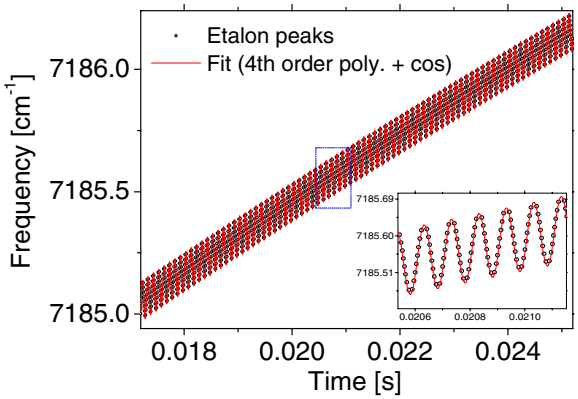

Figure 7. Measured frequency response to the laser injection-current-tuning and its best fit (same modulation configuration as figure 6).

simulated transmitted intensity versus time in terms of the incident intensity and absorbance:

$$ {}^{S}I_t(t) = {}^{M}I_0(t) \cdot \exp[-\alpha(\nu(t))], \tag{3}$$

where ${}^{M}I_0(t)$ is the intensity versus time of the modulated and scanned laser and was measured when the gas cell was empty (vacuum); $\nu(t)$ the laser wavelength-tuning characteristics including scan and modulation; and $\alpha(\nu(t))$ the absorption spectrum of the target gas in the region of the laser wavelength scan.

The absorption spectrum can be written as

$$\alpha(\nu(t)) = \exp\left(-\sum_j S_j \cdot \phi_j(\nu(t)) \cdot P \cdot x_i \cdot L\right), \tag{4}$$

where S_j and ϕ_j are the line strength and lineshape function of transition j; P is the total pressure of the gas; x_i is the mole fraction of absorber i; and L is the pathlength.

For this example, as well as many applications, the lineshape function is well described by a Voigt profile [39], which is a convolution of Doppler and collisional broadenings and depends on the Doppler and collision-broadened full-width at half-maximum given by equations (5) and (6), respectively:

$$\Delta\nu_D(\mathrm{cm}^{-1}) = 7.162 \times 10^{-7} \nu_0 \sqrt{T/M} \tag{5}$$

$$\Delta\nu_c(\mathrm{cm}^{-1}) = 2 \cdot P \cdot \sum_j x_j \cdot \gamma_j(T), \tag{6}$$

where M is the molecular mass (g); x_j is the mole fraction of collision partner j; and γ_j is the collisional broadening coefficient (cm^{-1} atm^{-1}) due to perturbation by the jth component. The relationship between γ_j and T can be described as

$$\gamma_j(T) = \gamma_j^{296\ \mathrm{K}} \cdot \left(\frac{296}{T}\right)^{n_j}, \tag{7}$$

where n_j is the temperature exponent of the collisional width.

Water vapor in this example is measured by scanning the laser over a pair of transitions, one near 7185.60 cm^{-1} (lower state energy, $E'' = 1045$ cm^{-1}) and its neighbor near 7185.39 cm^{-1} ($E'' = 447$ cm^{-1}). These transitions are overlapped by collisional broadening at atmospheric pressure

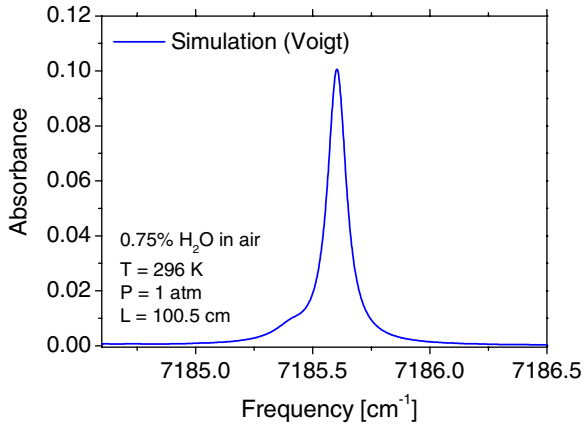

Figure 8. Simulated absorbance versus frequency for H_2O transition near 7185.6 cm^{-1} and its neighbor at 7185.39 cm^{-1} (0.75% H_2O in air, $P = 1$ atm, $T = 296$ K, $L = 100.5$ cm).

Table 1. Measured spectroscopic parameters for probed H_2O transition near 7185.60 cm^{-1} and its neighbor near 7185.39 cm^{-1} at 296 K.

Parameter	7185.60 cm^{-1}	7185.39 cm^{-1}
S (atm^{-1} cm^{-2})	0.0195	0.00 121
γ_{self} (cm^{-1} atm^{-1})	0.205	0.396
γ_{air} (cm^{-1} atm^{-1})	0.044	0.081

and provide a good test of the new WMS analysis method to recover the complex WMS lineshape for a pair of unresolved transitions. To accurately simulate the absorption spectrum for this example, the spectroscopic parameters including the line strength, H_2O–H_2O broadening (γ_{self}), and H_2O–Air broadening (γ_{air}) coefficients at 296 K were measured; the data are listed in table 1.

The absorption spectrum over the scan range shown in figure 8 was simulated with a Voigt lineshape at the measurement conditions ($P = 1$ atm, $T = 296$ K, $L = 100.5$ cm, 0.75% H_2O in air).

Using $\nu(t)$ from equation (2) and the simulated absorption spectrum in figure 8, the absorbance can be written as a function of time $\alpha(\nu(t))$ for the scanning and modulated laser. For this example $\alpha(\nu(t))$ for a single laser scan is illustrated in figure 9; note that the flat top of the absorbance is not saturation but is the modulation of the laser as its wavelength traverses the peak of the absorption seen in figure 9. The 25 Hz wavelength scan is slow enough compared to the 10 kHz modulation that the modulated wavelength includes the line center of the transition more than 20 times during the scan. Using equation (3) to combine the data for laser intensity versus time ${}^{M}I_0(t)$ from figure 6 with the absorbance versus time in figure 9, $\alpha(\nu(t))$, the simulated transmitted intensity versus time ${}^{S}I_t(t)$ can be calculated as shown in figure 10.

3.4. Lock-in analysis for WMS detection of H_2O

The measured and simulated transmitted laser intensities versus time were both numerically post-processed by using lock-in and finite-impulse-response (FIR) low-pass filter (bandwidth of 2 kHz) software. The transmitted intensities

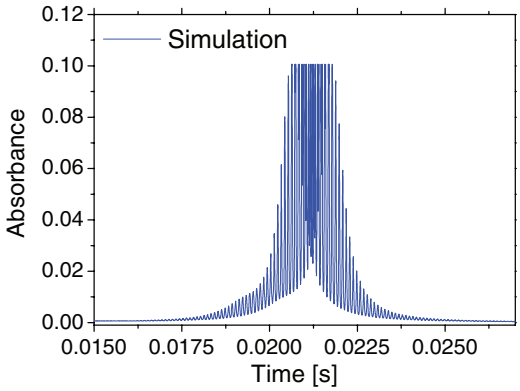

Figure 9. Simulated absorbance versus time $\alpha(t)$ for the H_2O transition near 7185.6 cm^{-1} (for the absorbance versus wavelength shown in figure 8). Note constant peak values between 0.021 and 0.0225 s are real (not detector saturation) as the modulation is fast compared to the scan rate.

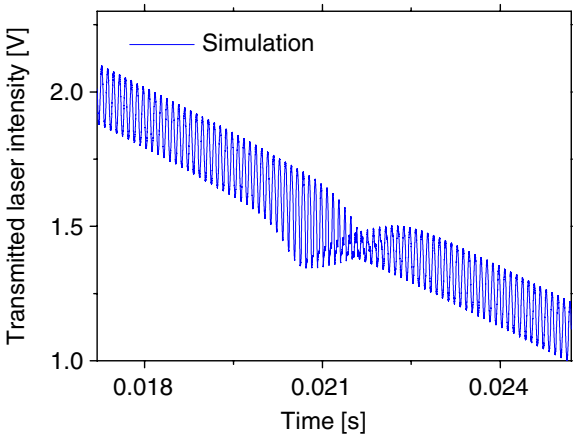

Figure 10. Simulated transmitted laser intensity versus time ${}^{s}I_t(t)$ for a single scan of the modulated laser over the absorption feature (for the laser intensity in figure 6 and the absorbance versus time in figure 9).

${}^{M}I_t(t)$ and ${}^{S}I_t(t)$ are each multiplied by $\cos(n \cdot 2\pi f t)$ (and $\sin(n \cdot 2\pi f t)$) to expand the X-component (and the Y-component) of the measured and simulated signals at each of the nf_m harmonics. A low-pass (LP) filter was used to extract these components by taking convolution, as

$$\begin{aligned} {}^{S}X_{nf}&: {}^{S}I_t(t) \cdot \cos(n \cdot 2\pi f_m t) \otimes \text{LP-filter} \\ {}^{M}X_{nf}&: {}^{M}I_t(t) \cdot \cos(n \cdot 2\pi f_m t) \otimes \text{LP-filter} \end{aligned} \quad (8)$$

$$\begin{aligned} {}^{S}Y_{nf}&: {}^{S}I_t(t) \cdot \sin(n \cdot 2\pi f_m t) \otimes \text{LP-filter} \\ {}^{M}Y_{nf}&: {}^{M}I_t(t) \cdot \sin(n \cdot 2\pi f_m t) \otimes \text{LP-filter}. \end{aligned} \quad (9)$$

Note the FIR low-pass filter bandwidth must be less than $f_m/2$ to avoid distorting the modulation and large enough to avoid distorting the wavelength-scanned WMS lineshape features (depends on scan range and rate, transition width and digitization rate). Because the simulated and measured signals use the same filter, any distortion will be common to

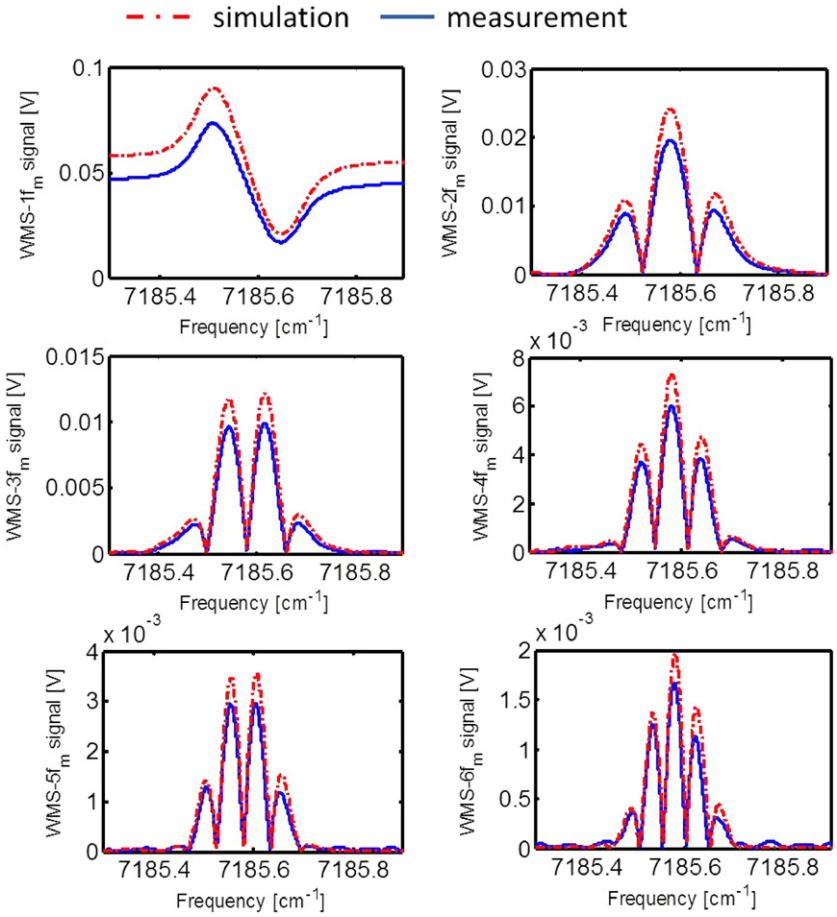

Figure 11. Measured and simulated WMS-nf_m spectra for H_2O transition near 7185.6 cm^{-1} (0.75% H_2O in air, $T = 296$ K, $P = 1$ atm, $L = 100.5$ cm, $a = 0.081$ cm^{-1}, $f_m = 10$ kHz, optical depth = 0.101). Note the amplitude difference was produced by attenuating the measurement laser intensity to mimic the influence of non-absorption losses.

both quantities. The absolute magnitude of the simulated and measured WMS-nf_m signals becomes

$$
\begin{aligned}
{}^{S}S_{nf} &= \sqrt{{}^{S}X_{nf}^{2} + {}^{S}Y_{nf}^{2}} \\
{}^{M}S_{nf} &= \sqrt{{}^{M}X_{nf}^{2} + {}^{M}Y_{nf}^{2}}.
\end{aligned}
\tag{10}
$$

Figure 11 shows the comparison between the simulated and measured WMS-nf_m signals (the time-cost for simulating each harmonic is ~0.1 s with a desktop computer (Dell XPS8500, CPU: i7-3770, 8 GB ram)); the shapes of each harmonic signal WMS-nf_m agree well between simulation and measurement but there is a significant difference in magnitude. The laser intensity for this demonstration measurement was reduced by a fiber attenuator added to simulate non-absorption laser intensity loss. The difference in magnitude between simulation and measurement in figure 11 with the fiber attenuator illustrates how each of the harmonic signals is proportional to laser intensity. The use of the attenuator to mimic non-absorption intensity loss provides an illustration of the use of WMS-$1f_m$-normalization of the other WMS-nf_m harmonic signals to account for time-varying laser intensity or non-absorption losses. Without the fiber attenuator there was no such difference between simulation and measurement illustrating the fidelity of this new scheme to simulate WMS-nf_m harmonics.

3.5. Issues for normalization by WMS-1f_m

The use of WMS-$1f_m$ to normalize the higher harmonics WMS-nf_m ($n \geqslant 2$) is well developed in the literature at line center [20–26]. However, the normalization of wavelength-scanned WMS has not previously been discussed. As seen in figure 11, the wavelength-scanned WMS-$1f_m$ signal is asymmetric with-respect-to the line center of the transition. Thus normalization will distort the WMS lineshapes; however, if this distortion is common to both simulation and measurement, quantitative fitting of the WMS lineshapes to determine gas parameters will still be possible [37]. As first noted by Cassidy and Reid [22] and described in detail in [40], the WMS-$1f_m$ signal has contributions from the laser intensity modulation and from the absorption by the target species. Here the highlights of the wavelength-scanned WMS-$1f_m$ lineshape are described to understand its use for WMS-nf_m normalization.

Figure 12 shows the wavelength-scanned WMS-$1f_m$ signal for the H_2O absorption demonstration at three optical depths (0.01, 0.1 and 1). For the optically thin case (0.01) the $1f_m$-signal shown by the solid black line in the

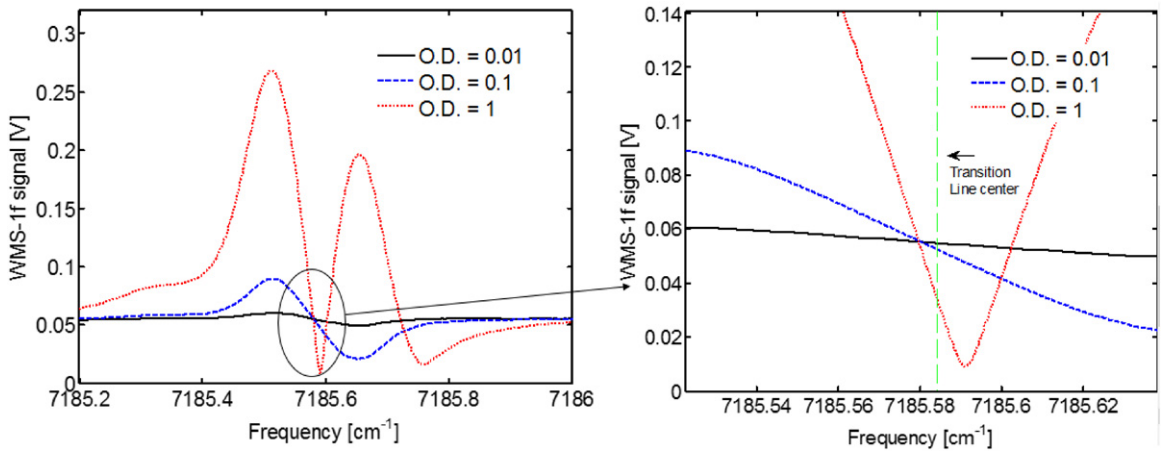

Figure 12. Simulated $1f_m$ spectra for H_2O transition near 7185.6 cm^{-1} at optical depths 0.01, 0.1 and 1.0 at 1 atm with a modulation index of 1.8 (the laser characterization is the same as figures 6 and 7; note the modulation index is 1.8, and the line center includes pressure shift in 1 atm air).

left panel of figure 12 is dominated by the amplitude of the laser intensity modulation. The value of the laser intensity modulation contribution to the WMS-$1f_m$ signal depends on the modulation depth and the laser intensity variation versus injection-current; larger modulation depth produces a larger WMS-$1f_m$ value at scan wavelengths away from the absorption transition.

As the optical depth increases the gas absorption contribution to the WMS-$1f_m$ signal increases and the blue dashed line in the left panel of figure 12 illustrates an optical depth of 0.1 (same as the experiment described in detail above and shown in figure 11). The asymmetric shape of the absorption contribution to the wavelength-scanned WMS-$1f_m$ signal becomes apparent. This asymmetric shape traces the first derivative of the absorption lineshape from figure 8.

For large optical depths attenuation of the WMS-$1f_m$ near line center must also be considered as illustrated by the inset in figure 12. The differences in the $1f_m$ signal at line center arises from the absorption of the laser intensity modulation contribution to the $1f_m$ signal, which increases with optical depth and decreases with wavelength modulation depth. WMS-$1f_m$ can be useful for the recovery of the absorption lineshape when the detector has large and or time-varying dark current, or if the application has significant optical emission. The use of WMS-$1f_m$ has been developed in the literature by workers at the University of Strathclyde [40, 41] and will not be discussed further here.

When the optical depth is increased even further, for example the red dot line in the left panel of figure 12, the absorption contribution to the $1f_m$ signal becomes larger than the contribution from the laser-modulation amplitude. Because WMS-nf_m harmonic signals are defined in equation (10) to always be greater than zero the $1f_m$ signal does not go negative, but it does approach near zero values at two wavelengths in the scan. Normalization by dividing by a signal with near-zero values, such as seen in the red dot–dashed curve in figure 12, can artificially weight only a few points in a fit of the $1f_m$-normalized WMS-nf_m lineshapes. For wavelength-scanned WMS at moderate optical depths, especially at large wavelength modulation depth, this issue can be avoided by normalization using the value for the mean WMS-$1f_m$ for each scan, which has proven quite effective for applications with large scattering losses such as coal-fired boiler exhaust [42] or coal gasification [43].

3.6. Normalization to account for non-absorption transmission losses

Even though the odd harmonics are asymmetric about the transition line center, all of the WMS-nf_m harmonics are proportional to laser intensity; thus the WMS-$1f_m$ signal can be used to normalize signals at other harmonics WMS-nf_m to account for non-absorption losses:

$$S_{nf}^{\text{normalized}} = S_{nf}/S_{1f}. \tag{11}$$

Figure 13 shows the WMS-$1f_m$-nomalized values of WMS-nf_m (n = 2–6) for the measured and simulated data from figure 11. The absorption component of the wavelength-scanned WMS-$1f_m$ signal in figure 11 is asymmetric with-respect-to the line center; thus, the $1f_m$-normalized wavelength-scanned WMS-nf_m lineshapes in figure 13 are distorted. The peak-signal for even harmonics of $1f_m$-normalized WMS-nf_m (n = 2, 4 and 6) are no longer at the line center of the transition (note the WMS-$2f_m$ peak signal is used to calibrate the laser wavelength scale and not the peak normalized signal). The WMS simulation scheme has the same normalization distortion as the measurement and thus, the simulations can be best fit to determine gas parameters [37]. The differences between simulations and measurements are also plotted as residuals in figure 12, and these values show agreement (defined as the ratio of the root mean square of the residual to the peak $1f$-normailized WMS-nf signals) within 3.2% for all harmonics from 2 to 6. The differences between simulation and measurement are dominated not by the differences in peak values, which differ by <1%, but are dominated by quite small differences in the wavelength scale between simulation and measurement. The fidelity of the demonstration measurement was limited by the wavelength scale and the digitizer time resolution. This

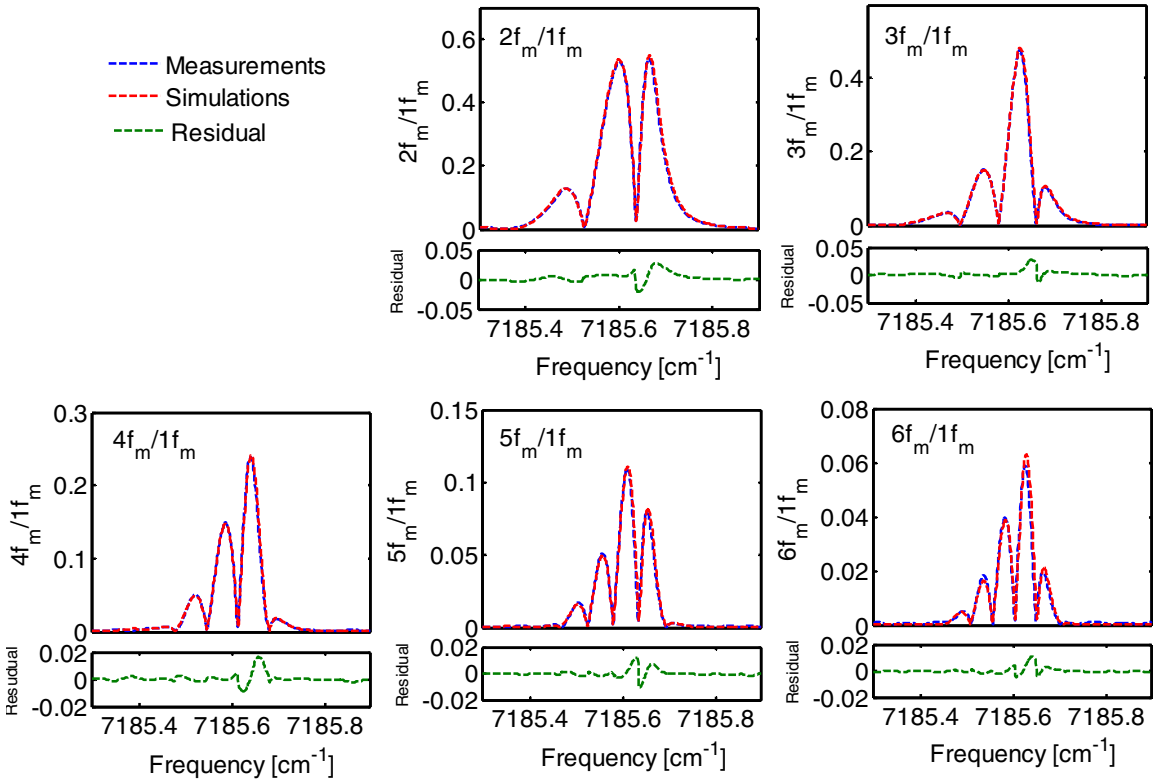

Figure 13. Measured and simulated $1f_{\mathrm{m}}$-normalized WMS-nf_{m} spectra for H_2O transition near 7185.6 cm^{-1} (same condition as figure 11, optical depth = 0.101).

demonstrates that the $1f_{\mathrm{m}}$-normalized WMS analysis provides an accurate WMS-nf_{m} lineshape for $n = 2$–6. Note the relative magnitude decreases as the harmonic increases. Additional digital resolution and perhaps an absorption lineshape more accurate than Voigt are needed to recover the lineshapes for WMS-nf_{m} harmonics for $n > 6$; for this demonstration experiment a 12 bit digitizer was used with a Voigt lineshape.

4. Comparison with Fourier analysis of WMS

The new WMS analysis method compares well with the established Fourier analysis approach as illustrated in the figure 14, which compares the H_2O demonstration measurement of the lineshape for $1f_{\mathrm{m}}$-normalized WMS-$2f_{\mathrm{m}}$ to that simulated using this approach and that simulated using traditional Fourier analysis where the intensity modulation is characterized only at transition line center [21, 25]. For this experiment with a relatively small modulation depth, a DFB single-mode laser with highly linear response to injection-current was used, and the two simulations are in good agreement with the measurements for the entire center lobe of the lineshape, and only disagree in the wings by ~10%. However, in the wings on either side of line center, the new analysis approach is in better than 1% agreement with the measurement for the entire lineshape. The match in simulation and measurement over the entire lineshape suggests the potential of fitting the $1f_{\mathrm{m}}$-normalized, wavelength-scanned WMS-nf_{m} lineshapes analogous to wavelength-scanned DA, and indeed research to investigate this approach is underway with promising results [37].

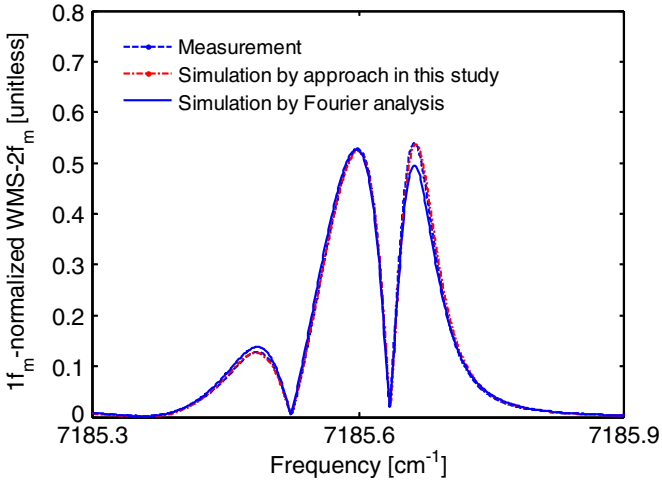

Figure 14. Comparison of the $1f_{\mathrm{m}}$-normalized WMS-nf_{m} spectra using different absorption analysis approaches for H_2O transition near 7185.6 cm^{-1} (same condition as figure 13).

5. Conclusions

A new method for the analysis of WMS absorption measurements using injection-current-modulated TDLs has been described in detail. Water vapor was detected via WMS near 7185.6 cm^{-1} in a static cell at 1 atm and 296 K using a distributed feedback (DFB) laser. WMS-nf_{m} harmonics for $n = 1$–6 were extracted and the $1f_{\mathrm{m}}$-normalized WMS-nf_{m} were in good agreement with the measurement over the entire WMS-nf_{m} lineshape.

This new analysis schemes differ from previous WMS analysis strategies in two significant ways: (1) the measured intensity of the wavelength-scanned, wavelength-modulated laser is used to simulate the transmitted laser intensity and (2) digital lock-in and low-pass filter software is used to expand both simulated and measured transmitted laser intensity into harmonics of the modulation frequency, WMS-nf_m (n = 1, 2, 3, . . .). This new approach has nine distinct advantages versus traditional analysis of WMS. (1) The use of measured laser intensity to simulate the Beer's law absorption signals avoids the need for an analytic model of laser intensity in its response to scanning and modulating the injection-current. (2) The use of measured intensity for the simulation also accounts for any wavelength-dependent transmission of other optical components in the apparatus. (3) The use of the digital lock-in and low-pass filter software to extract the WMS-nf_m harmonics from the simulated transmitted intensity avoids the complex Fourier expansion of the simulated absorption of the simultaneously scanned and modulated laser intensity and wavelength. (4) The scheme is valid for all WMS-nf_m harmonics, (5) at any optical depth, (6) at any modulation index, and (7) at all values of the mean laser wavelength even in the wings of the absorption away from line center. (8) This scheme is valid for WMS using unresolved blended transitions. (9) Using the same software for both simulation and measurement provides equal contributions of any non-ideal performance of the lock-in and low-pass filter software. We anticipate that this new analysis scheme will facilitate the development of robust wavelength-scanned WMS sensors for a wide range of practical absorption applications. Research is underway to investigate the extraction of gas parameters (concentration, temperature, pressure, collisional width, etc) from the best fit of wavelength-scanned WMS-nf_m lineshapes analogous to wavelength-scanned DA [37].

Acknowledgments

This work was supported by the National Energy Technology Laboratory of the Department of Energy, with Dr Susan Maley as the contractor monitor, and by the Air Force Office of Scientific Research, with Dr Chiping Li as the contract monitor.

References

[1] Hanson R K 2011 Applications of quantitative laser sensors to kinetics, propulsion and practical energy systems *Proc. Combust. Inst.* **33** 1–40

[2] Allen M G 1998 Diode laser absorption sensors for gas dynamic and combustion flows *Meas. Sci. Technol.* **9** 545–62

[3] Werle P 1998 A review of recent advances in semiconductor laser based gas monitors *Spectrochim. Acta* A **54** 197–236

[4] Wolfrum J 1998 Lasers in combustion: from basic theory to practical devices *Proc. Combust. Inst.* **27** 1–41

[5] Silver J A 1992 Frequency-modulation spectroscopy for trace species detection: theory and comparison among experimental methods *Appl. Opt.* **31** 707–17

[6] Hancock G, van Helden J H, Peverall R, Ritchie G A D and Walker R J 2009 Direct and wavelength modulation spectroscopy using a cw external cavity quantum cascade laser *Appl. Phys. Lett.* **94** 201110

[7] Meyer T R, Roy S, Anderson T N, Lucht R P, Jimenez R and Gord J R 2005 10 kHz detection of CO_2 at 4.5 μm by using tunable diode-laser-based difference-frequency generation *Opt. Lett.* **30** 3087–9

[8] Seiter M and Sigrist M W 1999 On-line multicomponent trace-gas analysis with a broadly tunable pulsed difference-frequency laser spectrometer *Appl. Opt.* **38** 4691–8

[9] Rieker G B, Jeffries J B, Hanson R K, Mathur T, Gruber M R and Carter C D 2009 Diode laser-based detection of combustor instabilities with application to a scramjet engine *Proc. Combust. Inst.* **32** 831–8

[10] Sanders S T, Baldwin J A, Jenkins T P, Baer D S and Hanson R K 2000 Diode-laser sensor for monitoring multiple combustion parameters in pulse detonation engines *Proc. Combust. Inst.* **28** 587–94

[11] Ebert V, Teichert H, Strauch P, Kolb T, Seifert H and Wolfrum J 2005 Sensitive *in situ* detection of CO and O_2 in a rotary kiln-based hazardous waste incinerator using 760 nm and new 2.3 μm diode lasers *Proc. Combust. Inst.* **30** 1611–8

[12] Deguchi Y, Noda M and Abe M 2002 Improvement of combustion control through real-time measurement of O_2 and CO concentrations in incinerators using diode laser absorption spectroscopy *Proc. Combust. Inst.* **29** 147–53

[13] Von Drasek W, Wehe S and Allen M 2004 Laser-based multiple gas species sensor for harsh combustion process control applications *Trends in Optics and Photonics, Conf. on Lasers and Electro-Optics* p 96

[14] Kosterev A A, Roller C, Tittel F K and Flory W 2003 Development of a QC-laser based system for industrial gas monitoring *OSA/CLEO Conf. on Lasers and Electro-Optics*

[15] Sur R, Sun K, Jeffries J B and Hanson R K 2013 Multi-species laser absorption sensors for *in-situ* monitoring of syngas composition *Appl. Phys.* B online, doi:10.1007/s00340-013-5567-2

[16] Reid J and Labrie D 1981 Second-harmonic detection with tunable diode lasers-comparison of experiment and theory *Appl. Phys.* B **26** 203–10

[17] Werle P 1996 Spectroscopic trace gas analysis using semiconductor diode lasers *Spectrochim. Acta* A **52** 805–22

[18] Sur R, Boucher T J, Renfro M W and Cetegen B M 2010 *In-situ* measurements of water vapor partial pressure and temperature dynamics in a PEM fuel cell *J. Electrochem. Soc.* **157** B45–53

[19] Chao X, Jeffries J B and Hanson R K 2009 Absorption sensor for CO in combustion gases using 2.3 μm tunable diode lasers *Meas. Sci. Technol.* **20** 115201

[20] Cassidy D T and Bonnell L J 1988 Trace gas detection with short-external-cavity InGaAsP diode laser transmitter modules operating at 1.58 μm *Appl. Opt.* **27** 2688–93

[21] Li H, Rieker G B, Liu X, Jeffries J B and Hanson R K 2006 Extension of wavelength-modulation spectroscopy to large modulation depth for diode laser absorption measurements in high-pressure gases *Appl. Opt.* **45** 1052–61

[22] Cassidy D T and Reid J 1982 Atmospheric pressure monitoring of trace gases using tunable diode lasers *Appl. Opt.* **21** 1185–90

[23] Fernholz T, Teichert H and Ebert V 2002 Digital, phase-sensitive detection for *in situ* diode laser spectroscopy under rapidly changing transmission conditions *Appl. Phys.* B **75** 229–36

[24] Sun K, Chao X, Sur R, Jeffries J B and Hanson R K 2013 Wavelength modulation diode laser absorption spectroscopy for high pressure gas sensing *App. Phys.* B **110** 497–508

[25] Rieker G B, Jeffries J B and Hanson R K 2009 Calibration-free wavelength-modulation spectroscopy for measurements of gas temperature and concentration in harsh environments *Appl. Opt.* **48** 5546–60
[26] Uehara K and Tai H 1992 Remote detection of methane with a 1.66-μm diode laser *Appl. Opt.* **31** 809–14
[27] Dharamsi A N 1996 A theory of modulation spectroscopy with applications of higher harmonic detection *J. Phys. D: Appl. Phys.* **29** 540–9
[28] Kluczynski P, Gustafsson J, Lindberg A M and Axner O 2001 Wavelength modulation absorption spectrometry—an extensive scrutiny of the generation of signals *Spectrochim. Acta* B **56** 1277–354
[29] Schilt S, Thevenaz L and Robert P 2003 Wavelength modulation spectroscopy: combined frequency and intensity laser modulation *Appl. Opt.* **42** 6728–38
[30] Wilson G V H 1963 Modulation broadening of NMR and ESR line shapes *J. Appl. Phys.* **34** 3276–85
[31] Philippe L C and Hanson R K 1993 Laser diode wavelength-modulation spectroscopy for simultaneous measurement of temperature, pressure, and velocity in shock-heated oxygen flows *Appl. Opt.* **32** 6090–103
[32] Kluczynski P, Lindberg A M and Axner O 2004 Wavelength modulation diode laser absorption signals from Doppler broadened absorption profiles *J. Quant. Spectrosc. Radiat. Transfer* **83** 345–60
[33] Arndt R 1965 Analytical line shapes for Lorentzian signals broadened by modulation *J. Appl. Phys.* **36** 2522–4
[34] Axner O, Kluczynski P and Lindberg A M 2001 A general noncomplex analytical expression for the *n*th Fourier component of a wavelength-modulated Lorentzian line-shape function *J. Quant. Spectrosc. Radiat. Transfer* **68** 299–317
[35] Chao X, Jeffries J B and Hanson R K 2012 Wavelength-modulation-spectroscopy for real-time, *in situ* NO detection in combustion gases with a 5.2 μm quantum-cascade laser *Appl. Phys.* B **106** 987–97
[36] Strand C L and Hanson R K 2011 Thermometry and velocimetry in supersonic flows via scanned wavelength-modulation absorption spectroscopy *47th AIAA/ASME/SAE/ASEE Joint Propulsion Conf. and Exhibition* AIAA 2011-5600
[37] Goldenstein C S, Strand C L, Schultz I A, Sun K, Jeffries J B and Hanson R K 2013 Fitting of calibration-free scanned-wavelength-modulation spectroscopy spectra for determination of gas properties and absorption lineshapes *Appl. Opt.* submitted
[38] Rothman L S, Gordon I E, Barber R J, Dothe H, Gamache R R, Goldman A, Perevalov V, Tashkun S A and Tennyson J 2010 HITEMP, the high-temperature molecular spectroscopic database *J. Quant. Spectrosc. Radiat. Transfer* **111** 2139–50
[39] Mclean A B, Mitchell C E J and Swanston D M 1994 Implementation of an efficient analytical approximation to the Voigt function for photoemission lineshape analysis *J. Electron Spectrosc.* **69** 125–32
[40] Stewart G, Johnstone W, Bain J R, Ruxton K and Duffin K 2011 Recovery of absolute gas absorption line shapes using tuneable diode laser spectroscopy with wavelength modulation—part I: theoretical analysis *J. Lightwave Technol.* **29** 811–21
[41] Bain J R P, Johnstone W, Ruxton K, Stewart G, Lengden M and Duffin K 2011 Recovery of absolute gas absorption line shapes using tuneable diode laser spectroscopy with wavelength modulation—part 2: experimental investigation *J. Lightwave Technol.* **29** 987–96
[42] Chao X, Jeffries J B and Hanson R K 2013 Real-time, *in situ*, continuous monitoring of CO in a pulverized coal-fired power plant with a 2.3 lm laser absorption sensor *Appl. Phys.* B **110** 359–65
[43] Sun K, Sur R, Chao X, Jeffries J B, Hanson R K, Pummill R J and Whitty K J 2013 TDL absorption sensors for gas temperature and concentrations in a high-pressure entrained-flow coal gasifier *Proc. Combust. Inst.* **34** 3593–601